Preprint version

The 3D construction of leaves is coordinated with water use efficiency in conifers.

Santiago Trueba[1,2,*], Guillaume Théroux-Rancourt[3], J. Mason Earles[4], Thomas N. Buckley[5], David Love[6], Daniel M. Johnson[6], Craig Brodersen[1].

[1] *School of the Environment, Yale University, New Haven, CT, USA.*
[2] *University of Bordeaux, INRAE, BIOGECO, Pessac, France.*
[3] *Institute of Botany, University of Life Sciences and Natural Resources, Vienna, Austria.*
[4] *Department of Viticulture and Enology, University of California Davis, CA, USA.*
[5] *Department of Plant Sciences, University of California Davis, CA, USA.*
[6] *Warnell School of Forestry and Natural Resources, University of Georgia, GA, USA.*

[*]Corresponding author: strueba@gmail.com

Abstract

Conifers dominate the canopies of many terrestrial biomes, holding a great ecological and economic importance globally. Current increases in temperature and aridity are resulting in conifer mortality and imposing high transpirational demands to global vegetation. Therefore, identifying leaf structural determinants of carbon acquisition and water use efficiency is essential in predicting physiological impacts due to environmental variation. Using synchrotron-generated microCT imaging, we extracted leaf volumetric anatomy and stomatal traits in 34 species across the conifers with a special focus on *Pinus*, the richest conifer genus. We show that intrinsic water use efficiency (WUE_i) is driven by leaf vein volumetrics, with both traits scaling positively. The ratios of stomatal pore number per unit mesophyll or intercellular airspace volume emerged as powerful explanatory variables, accurately predicting both stomatal conductance and WUE_i. Our results clarify how the three-dimensional organization of tissues within the leaf has a direct impact on plant water use and carbon uptake.

Keywords: gas exchange, gymnosperm, leaf anatomy, leaf ecophysiology, stomatal conductance, stomatal density.

Introduction

Conifer forests thrived on the earth surface during the Mesozoic until the radiation and diversification of angiosperms during the Cretaceous, which was followed by angiosperm ecological dominance attributed to increased physiological performance and reduced generation times [1-4]. Yet, after 100 million years of competition with the angiosperms, conifers remain dominant in the canopy of many biomes [5]. Conifers are found in ecosystems from high latitudes to the equator, and they have a major economic importance in the wood and paper industries [6]. Conifer-dominated forests are not exempt from the impacts of drought and aridity resulting from ongoing global climatic changes [7-9]. This is particularly alarming given that 48% of the 722 conifer taxa of the world are currently threatened [10]. Global increases in temperature coupled with rising vapor pressure deficit (VPD) place increased strain on plant hydraulic and photosynthetic systems [11,12]. There is strong evidence showing that water use efficiency (WUE) has increased in recent decades, most probably because of rising CO_2 levels [13,14]. However, the physiological mechanisms behind this trend need to be further elucidated [15], and there is still a lack of knowledge on how leaf structural organization is coupled with key functions such as photosynthetic carbon acquisition, stomatal conductance, and the interplay between both driving intrinsic water use efficiency (WUE_i).

Leaf-level photosynthetic metabolism has an important role in maintaining global ecological processes [16]. Therefore, exploring tissue organization inside the leaf, and specifically the mesophyll cells where water and gas diffusion occurs, is important for understanding carbon, water, and energy fluxes at whole ecosystem levels. The leaf mesophyll consists of photosynthetic parenchyma cells located between the epidermis and bundle sheath layers. Once inside the leaf, the diffusion of CO_2 through the intercellular airspace (IAS) and to the chloroplasts (i.e. mesophyll conductance) is a major constraint on photosynthetic performance [17,18]. This pathway includes the IAS, but also the diffusion of CO_2 across mesophyll cell walls, cell membranes, and the chloroplast envelope, which can significantly limit photosynthesis in gymnosperms [19]. Previous work has shown that mesophyll surface area per leaf area (S_m; μm^2 μm^{-2}) had a strong influence on maximum photosynthesis [20,21]. More recently, it has been suggested that the surface area of the mesophyll exposed to the IAS per unit of mesophyll

volume (SA_{mes}/V_{mes}; $\mu m^2\ \mu m^{-3}$) can influence plant photosynthetic performance given that the mesophyll-IAS boundary is the primary interface between the atmosphere and the photosynthetic cells [22,23]. Other volumetric anatomical traits such as mesophyll porosity (i.e. IAS as a fraction of total mesophyll volume; $\mu m^3\ \mu m^{-3}$) might be relevant in promoting diffusion through the IAS, and it has been suggested that mesophyll palisade porosity is correlated to stomatal conductance across four different *Arabidopsis* mutants [24]. The relevance of such anatomical traits arises from the hypothesis that photosynthetic capacity could be enhanced by increasing surface area of mesophyll exposed to the IAS, allowing for more potential surface for CO_2 diffusion into chloroplasts, across mesophyll cell walls, and chloroplast envelopes [22,25]. However, the correct estimation of such anatomical traits using standard two-dimensional (2D) techniques is difficult since it relies on 2D approximations of the complex, three-dimensional (3D) shape of the mesophyll [26,27].

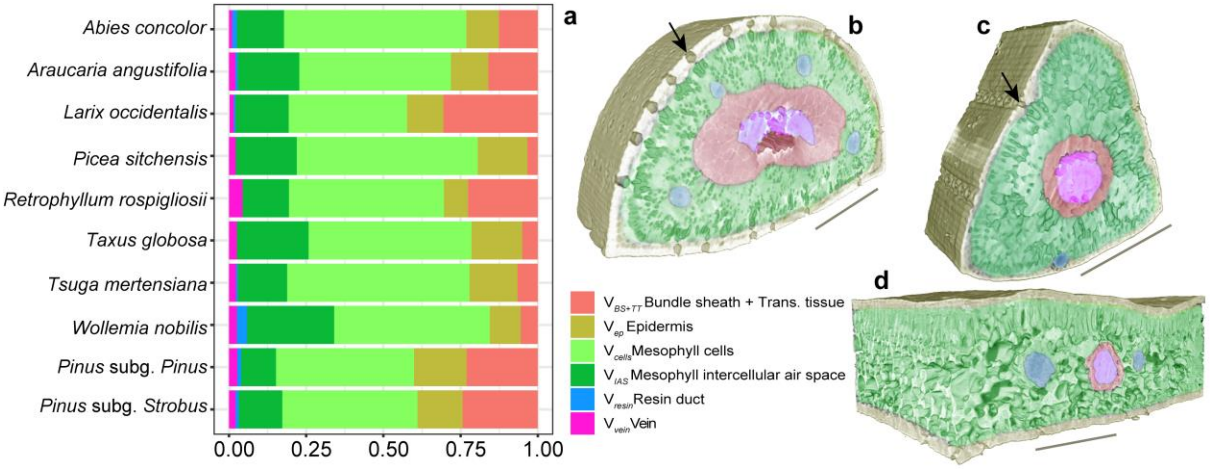

Figure 1. Proportion of different tissue volumes relative to total leaf volume inside the 3D leaf space in conifers (a). Average values of *Pinus* species belonging to the *Pinus* subgenus (21 spp) and *Strobus* (5 spp) are included. MicroCT 3D images of *Pinus pungens* (b; *Pinus* subgenus), *Pinus monticola* (c; *Strobus* subgenus) and *Wollemia nobilis* (d). Segmented tissues are indicated with different colors and stomatal apertures are indicated with arrows. Scale bars = 250 µm. A plot including all 34 species is available in Supplementary Fig. 2.

Three-dimensional volumetric images of the leaf structure can be obtained through X-ray micro-computed tomography (microCT), opening new research avenues by allowing direct 3D estimations of important features such as the structure of the photosynthetic tissue [26,27]. However, leaf volumetric traits other than those relative to the mesophyll might also influence CO_2 and

water diffusion inside the conifer leaf. Comprehensive investigations of 3D structural variability encompassing several leaf tissues are therefore needed. Given the elementary vascular architecture of the conifer leaf (Fig. 1), which typically consists of a single vein without further branching [28,29], and the mechanistic link between hydraulic conductance and maximum photosynthetic rates [30], we predict that higher volumes of vascular tissue per unit leaf volume (V_{vein}/V_{leaf}; $\mu m^3\ \mu m^{-3}$) should be a good predictor of gas exchange and WUE_i. We also predict a positive relationship between gas exchange efficiency and the ratio of mesophyll surface area exposed to the IAS and vein volume (SA_{mes}/V_{vein}; $\mu m^2\ \mu m^{-3}$), where a greater investment in vein volume per unit area of bulk tissue surface should increase the hydraulic capacity to replace water lost to transpiration. In conifer leaves, water moves across the bundle sheath and the transfusion tissue before reaching the mesophyll [31]. Therefore, bundle sheath and transfusion tissue volume relative to total leaf volume (V_{BS+TT}/V_{leaf}; $\mu m^3\ \mu m^{-3}$), should also influence the efficiency of water movement within the leaf. Along with the previously described features, many conifer species also possess resin ducts, which play a major role in chemical and physical defense [32,33], but necessarily displace vascular or photosynthetic tissue, incurring both maintenance and construction costs, but also lost opportunity costs for net carbon gain. Finally, water movement inside the leaf ends at the stomatal pores, which play a major role in regulating water loss and maintaining water status in conifers [34]. Within this context, it is possible to determine the proportionality of different anatomical traits, the coordination between supply and demand for CO_2 and H_2O, and the physical constraints of leaf construction. To probe these relationships, we describe how conifers build their elementary, yet diverse leaves, and how structural features relate to key physiological traits.

This study presents an extensive survey of the three-dimensional organization (Supplementary Table 1) of the conifer leaf using microCT imaging. Our study includes 34 conifer species (Supplementary Fig. 1), with a special focus on the genus *Pinus*, the largest extant genus of conifers [35]. *Pinus* species can be found in a broad range of environmental conditions, suggesting wide structural and functional diversity [36]. *Pinus* subgenera *Pinus* and *Strobus* can be distinguished by having two or one vascular bundles respectively, centrally located inside the leaf [35] (Figs. 1a-c). Given that the vascular system appears to be relatively fixed, a central question is whether the non-vascular tissues show greater variability. We

hypothesize that features enhancing mesophyll surface area for gas diffusion will be positively correlated with the light-saturated assimilation rate of CO_2 (A_{sat}) and maximal stomatal conductance (g_{smax}). We provide an original assessment of the ratio of stomatal number and mesophyll volumetric features, expecting that leaves having less mesophyll volume per number of stomata will have higher rates of gas exchange and WUE_i due to an enhancement of the epidermal pores serving as evaporative surface relative to the photosynthetic tissue.

Results

The mesophyll (V_{mes}/V_{leaf}), including cells and airspace, represents the dominant leaf volume fraction for all measured species, occupying an average of 60% of the total leaf volume (Fig. 1; Supplementary Fig. 2). Depending on the species, the second largest volume fraction was either the combined bundle sheath and transfusion tissue volume (V_{BS+TT}/V_{leaf}) or the epidermis (V_{ep}/V_{leaf}), which represented an average of 22% and 16% of the leaf volume, respectively (Fig. 1a). Veins (V_{vein}/V_{leaf}) and resin ducts (V_{resin}/V_{leaf}) represented the smallest fraction of the total leaf volume (Fig. 1a), and resin ducts were completely absent in six measured species. V_{vein}/V_{leaf} was remarkably variable with 30-fold variation ranging from 0.002 $\mu m^3\ \mu m^{-3}$ in *Larix occidentalis* to 0.06 $\mu m^3\ \mu m^{-3}$ in *Pinus jeffreyi*. Across conifer species, V_{vein}/V_{leaf} had a mean value of 0.02 ± 0.002 $\mu m^3\ \mu m^{-3}$. Mesophyll porosity ranged from 0.15 $\mu m^3\ \mu m^{-3}$ in *Pinus pungens* (Fig. 1b) to 0.36 $\mu m^3\ \mu m^{-3}$ in *Wollemia nobilis* (Fig. 1d). Mean mesophyll porosity across species was 0.23 ± 0.01 $\mu m^3\ \mu m^{-3}$. SA_{mes}/V_{mes} had a mean value of 0.12 ± 0.01 $\mu m^2\ \mu m^{-3}$ and ranged from 0.06 $\mu m^2\ \mu m^{-3}$ to 0.20 $\mu m^2\ \mu m^{-3}$ in *Araucaria angustifolia* and *Pinus halepensis*, respectively. SA_{mes}/V_{vein} ranged from 1.16 $\mu m^2\ \mu m^{-3}$ in *Pinus pinea* to 36.61 $\mu m^2\ \mu m^{-3}$ in *Larix occidentalis* and had a mean value of 5.26 ± 1.11 $\mu m^2\ \mu m^{-3}$. The mesophyll surface area per total leaf area, S_m, ranged from 3.51 $\mu m^2\ \mu m^{-2}$ in *Pinus fenzeliana* to 24.91 $\mu m^2\ \mu m^{-2}$ in *Taxus globosa*, and had a mean value of 11.27 ± 0.79 $\mu m^2\ \mu m^{-2}$. We found structural coordination amongst volumetric anatomy traits (standard major axes; Supplementary Table 2). For instance, a negative allometric scaling between V_{ep}/V_{leaf} and V_{mes}/V_{leaf} was observed ($r^2 = 0.27$, $p < 0.01$), indicating that increasing the relative allocation to the mesophyll was done in conjunction with a decrease in the relative allocation to the epidermis. Average values of all measured volumetric traits are included in Supplementary Dataset 1 (available on request).

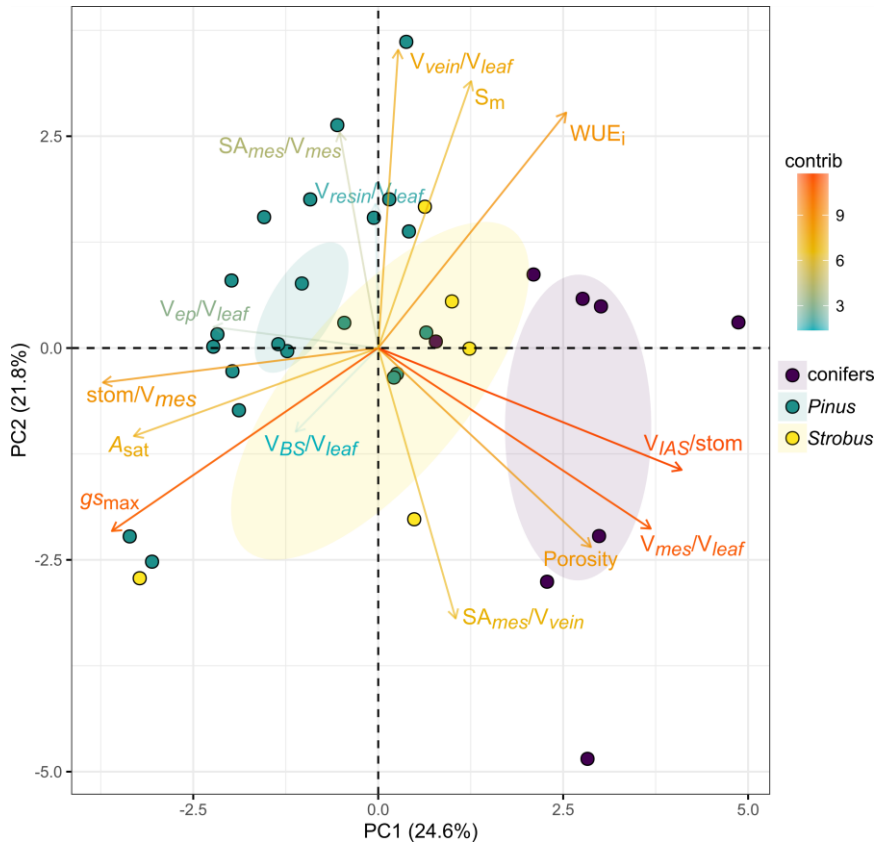

Figure 2. Principal component analysis (PCA) of physiological and volumetric anatomical traits for 34 conifer species. Arrows and trait color gradients indicate the contribution of each variable to the axes. Species from the two *Pinus* subgenera, along with other studied conifer species are indicated in different colors, and 95% confidence ellipses are included.

A multivariate analysis of trait covariation on 14 selected variables defined two major axes explaining 48% of inertia (Fig. 2). Inertia of the first axis was mainly explained by V_{IAS}/stomate (18.27%), stomata/V_{mes} (15.04%), V_{mes}/V_{leaf} (14.74%) and g_{smax} (14.08%). Increasing g_{smax} was associated on the first axis with increases in stomata/V_{mes} and A_{sat}, and decreases in mesophyll porosity, V_{mes}/V_{leaf}, and V_{IAS}/stomate (Fig. 2). The second axis was largely explained by V_{vein}/V_{leaf} (18.04%), SA_{mes}/V_{vein} (14.83%) and S_m (14.45%). Increasing WUE_i was associated on the second axis with increases in S_m and V_{vein}/V_{leaf}, and decreases in stomata/V_{mes} (Fig. 2). Conifer species were dispersed along both major axes. Non-*Pinus* conifer species were segregated on the first axis due to their higher porosity (Fig. 1d), V_{mes}/V_{leaf}, and V_{IAS}/stomate values, while species from the *Pinus* subgenus were grouped due to higher V_{ep}/V_{leaf} (Fig. 1b), along with a relatively larger SA_{mes}/V_{mes}. Species from the *Strobus* subgenera were

located between the previously described conifer groups (Fig. 2). The divergent distribution of species belonging to different conifer clades in the PCA analysis was further supported with one-way ANOVA analyses on leaf volumetric anatomy traits and stomatal density (Fig. 3; Supplementary Table 3).

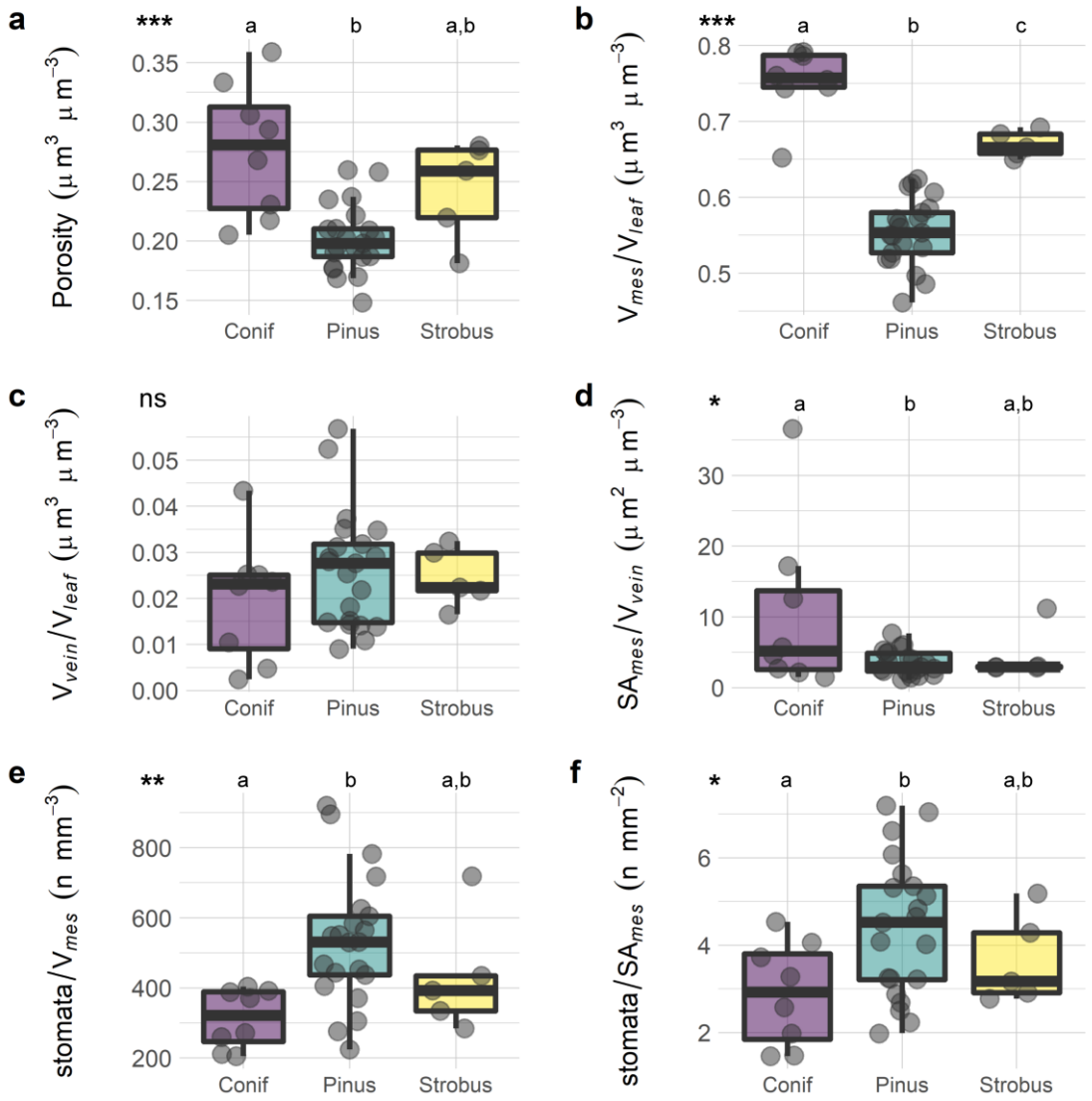

Figure 3. Comparison of volumetric anatomy (a-d) and stomatal density (e,f) between the *Pinus* subgenera *Pinus* and *Strobus* and other conifer species studied. Boxes and bars show the median, quartiles, and extreme values. Gray dots are species data points. *P*-values notations represent results of one-way ANOVAs between groups. ns: non-significant; * $p \leq 0.05$; ** $p \leq 0.01$; *** $p \leq 0.001$. Letters indicate significant differences between groups. Further information and other comparisons of traits between groups are available in Supplementary Table 3.

Mesophyll porosity and V_{mes}/V_{leaf} were amongst the most divergent traits across groups (Figs. 1,3; Supplementary Table 3), where non-*Pinus* conifer species showed significantly higher porosities and V_{mes}/V_{leaf} (Figs. 1d; 3a,b), while species from the *Pinus* subgenus showed the least porous and voluminous mesophylls (Figs. 1b; 3a,b). Relative vein volume was highly conserved across conifer groups (Fig. 3c), whereas mesophyll surface area per vein volume, along with traits related to the interaction of stomatal number and mesophyll tissue volumes showed significant differences across clades (Fig. 3d-f; Supplementary Table 3).

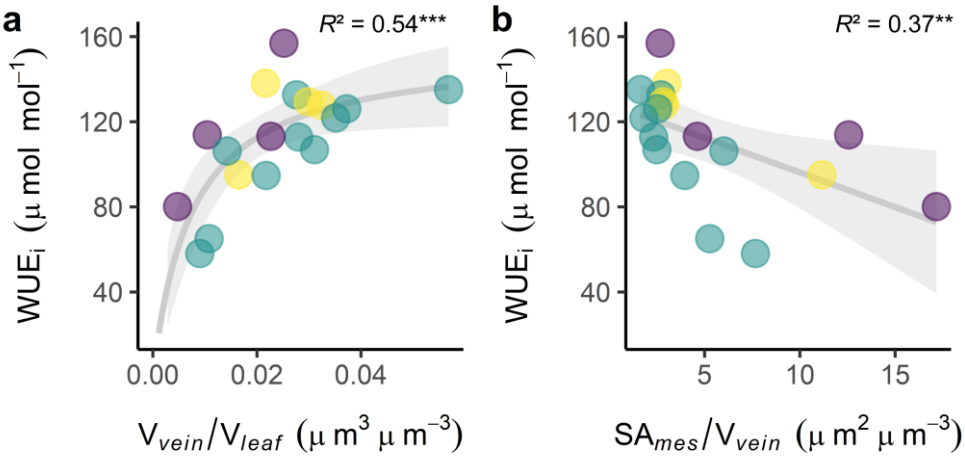

Figure 4. Water use efficiency (WUE_i) as a function of vein volumetric traits of conifer leaves. Relationships of WUE_i with relative vein volume (a) and the surface area of the mesophyll exposed to the IAS per unit of vein volume (b) across 18 conifer species. Solid regression lines and 95% confidence intervals are included. *Pinus* species from the subgenera *Pinus* (green circles) and *Strobus* (yellow circles), along with other conifer species (purple circles) are indicated. PGLS coefficients of determination are included. ** $p < 0.01$; *** $p < 0.001$. Additional information available in Supplementary Table 4.

To explore the functional implications of 3D tissue configuration, we determined their relationships to gas exchange parameters such as A_{sat}, g_{smax}, and WUE_i. WUE_i was best predicted by V_{vein}/V_{leaf} (Fig. 4a), showing that higher V_{vein}/V_{leaf} enhances leaf WUE_i. Further, 2D anatomical estimations of the ratio A_{vein}/A_{leaf} were comparable to V_{vein}/V_{leaf}, extracted using a 3D approach (Supplementary Text 1; Supplementary Fig. 3). The mesophyll surface area exposed to vein volume was also an accurate predictor and showed a negative relationship with WUEi (Fig. 4b). A significant relationship of WUE_i with S_m was also found using generalized least-square models corrected for phylogenetic relatedness (PGLS) analyses (Supplementary Table 4). A_{sat} was the physiological trait showing the least linkage with 3D structural traits. However, we found a negative relationship between A_{sat} and mesophyll porosity along with V_{mes}/V_{leaf} (Supplementary Table 4; Supplementary Fig. 4a), suggesting

that conifer species with lower relative mesophyll volumes have greater photosynthetic assimilation rates. Additionally, V_{IAS}/stomate was also negatively related to A_{sat} (Supplementary Fig. 4b). The number of stomata per unit mesophyll tissue volume predicted g_{smax} and WUE_i well (Fig. 5, Supplementary Table 4). For instance, high stomatal numbers relative to mesophyll volume (stomata/V_{mes}) enhanced g_{smax} (Fig. 5a) while decreasing WUE_i (Fig. 5b). Evolutionary coordination between leaf volumetric anatomy and physiological traits was supported by PGLS analyses (Supplementary Table 4). Stomatal density measured on a 2D leaf surface area basis, included here as a reference of a more standard approach, did not relate to any physiological trait (Supplementary Table 4). Therefore, the interaction of mesophyll volume and stomatal numbers emerged as a key trait to explain leaf physiological performance (Fig. 5). A comparison of the studied conifers with published data for other gymnosperm species, along with angiosperms and ferns, showed that conifers had fewer stomata per unit mesophyll volume than angiosperms *sensu largo* (Supplementary Fig. 5; Supplementary Dataset 2, available on request). However, this difference was less important when considering evergreen angiosperms alone. Conifers showed a similar stomata/V_{mes} ratio as other gymnosperm species and ferns (Supplementary Fig. 5).

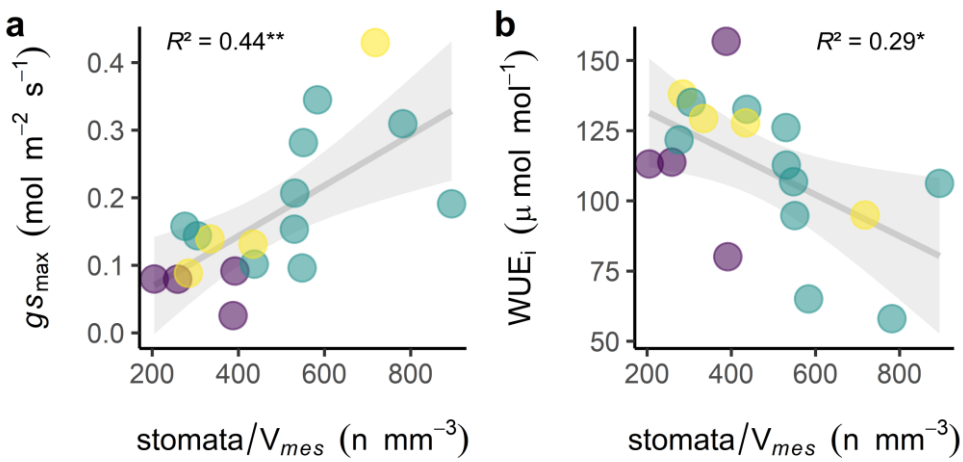

Figure 5. Physiological traits explained by stomatal traits in combination with volumetric anatomy in conifer leaves. Relationships of maximum stomatal conductance (a) and water use efficiency (b) with the number of stomata per unit of mesophyll volume across 18 conifer species. Solid regression lines and 95% confidence intervals are included. *Pinus* species from the subgenera *Pinus* (green circles) and *Strobus* (yellow circles), along with other conifer species (purple circles) are indicated. PGLS coefficients of determination are included. * $p < 0.05$; ** $p < 0.01$. Additional information available in Supplementary Table 4.

Discussion

Conifers, with their long-lasting and anatomically elementary leaves, must rely on leaf construction to enable sufficient carbon assimilation to survive and reproduce while limiting water loss. However, conifer needles have been considered to have a poor, if not absent, hydraulic connection between the vein xylem and the bulk leaf tissue [37]. This is unsurprising since conifer leaves are not as fully vascularized as those of angiosperms and present a single cohort of relatively inefficient leaves [4]. The likely consequence of this poor hydraulic connection is a larger difference in water potential between the veins and the mesophyll and epidermis in transpiring leaves, which may force stomata to close even when water potential is relatively high in the veins [37]. Our results show that despite occupying a small fraction (ca. 2%) of the leaf volumetric matrix, vein tissue volume has a great impact on the leaf WUE_i (Fig 3a). As the vein volume expands, the space between the vascular tissues and the bulk leaf tissues become smaller, potentially reducing the hydraulic resistance for water transport from the vasculature to the bulk leaf. Our study provides an original estimation of the full volumetric space occupied by the vein tissue. Yet, we found that standard 2D anatomical estimations of the relative surface covered by veins over a few leaf cross sections could be accurately employed to predict the vein volumetric fraction, and in turn water use efficiency in conifer leaves (Supplementary Text 1; Supplementary Fig. 3). Stomatal and venation densities covary in angiosperms, directly affecting gas exchange and water use capacities [38]. However, conifers do not provide a dense network of veins within the mesophyll to irrigate the photosynthesizing cells in water. Consequently, conifers might be constrained to increase the relative volume of veins as a single way to provide more water to the leaf.

Previous work has suggested that narrow leaves in conifers, which is a common feature in the Pinaceae [29,39], would be a response to alleviate their lack of hydraulic ramification. With the photosynthetic tissue encircling the single vascular cylinder, the distance from the vein to the epidermis largely sets hydraulic conductance outside the xylem, and leaf width becomes a major limiting factor in cylindrical, narrow leaves. Increasing the radial pathlength for water transport should effectively limit leaf hydraulic conductance, in turn limiting photosynthetic rates [29]. Our data support this hypothesis, with a negative relationship between mesophyll volume and A_{sat} (Supplementary Fig. 4a; Supplementary Table 4). Thus, within our dataset we find evidence for a significant photosynthetic penalty for increasing leaf width and mesophyll volume. With a limited ability to maximize

photosynthetic capacity through hydraulic ramification, the cylindrical needle may offer opportunities for other structural elements that allow improved hydraulic performance. Accessory transfusion tissue is one of them, where specialized cells connect the veins and/or bundle sheath to the mesophyll tissue, providing more water to the photosynthesizing cells and improving hydraulic contact to the epidermis [40]. This might lead to increased photosynthetic rates and WUE. However, we did not find a direct linkage of the combined volumes of bundle sheath and transfusion tissue with any measured physiological trait (Supplementary Table 4). It has been stated that reaching high photosynthetic rates requires high leaf porosity values, which increase CO_2 diffusion [7]. Yet, we observed a different trend with a negative relationship between mesophyll porosity and A_{sat} (Supplementary Table 4). Moreover, A_{sat} was strongly negatively related with V_{mes}/V_{leaf} in our dataset (Supplementary Fig. 4a). Previously, a decline of illumination-induced fluorescence as a function of leaf depth was observed in two conifers with needle-like leaves [41]. Therefore, the decrease of A_{sat} in leaves with more voluminous mesophylls might be explained by a limitation of light propagation across the mesophyll. Interestingly, we found conspicuous differences in leaf design between both *Pinus* subgenera and other conifers (Figs. 1;2;3a,b; Supplementary Table 3), with narrow needle-leaved *Pinus* possessing less voluminous and porous mesophylls. Such differences in mesophyll construction could explain why A_{sat} was greatest in *Pinus* species (Supplementary Table 3).

SA_{mes}/V_{vein} is another feature that diverged between conifer clades (Fig. 3d; Supplementary Table 3). We propose SA_{mes}/V_{vein} as another anatomical organization involved in regulating the control over the loss of water (Fig. 4b). Minimizing this ratio would mean that less surface is available for evaporation for a given vein water volume, thus increasing the time before this capacitor is depleted, thereby lowering the 'safety margin' between stomatal closure and xylem cavitation [37]. Also, in the context of poorly connected hydraulic design, decreasing SA_{mes}/V_{vein} would minimize the apoplastic surface for water to travel from the vein to the epidermis, hence by proxy decreasing the water path length and increasing connectivity to the epidermis to allow stomata to stay open longer and photosynthesis to continue. In our dataset, decreasing SA_{mes}/V_{vein} was achieved mainly by increasing the relative volume of veins, i.e. investing more in vascular tissue (Fig. 4). The relative benefit of investing in vein volume to increase the efficiency in water use seems to plateau above ~3% of leaf volume, and most species produce invests in veins close to that relative volume (Fig. 4a). *Pinus* species have in addition decreased the relative volume of the mesophyll by

decreasing airspace volume (Figs. 1; 3a) with plicate mesophyll cells [42]. Decreasing porosity leads to more cells being in contact with each other, thereby decreasing SA_{mes}, i.e. the surface of cells exposed to the IAS. Increasing IAS had a positive effect on WUE in six angiosperm species [43]. Although positive, we could not find a significant relationship between mesophyll porosity and WUE_i in conifer leaves (Supplementary Table 4). Beyond considering mesophyll features alone, mesophyll volumetrics in interaction with stomatal pore number emerged here as key traits to explain conifer gas exchange and WUE_i (Fig. 5; Supplementary Table 4). Using *Arabidopsis* and wheat as model plants, it has been suggested that stomatal differentiation during leaf development might induce mesophyll airspace formation [24]. Our study shows that this coordination between V_{IAS}, along with V_{mes}, and stomatal number have a significant impact on carbon assimilation and gas exchange on conifers (Fig. 5; Supplementary Table 4), further supporting this crucial linkage. Considered in a wider context, our observations might provide a novel structural basis to explain the lower photosynthetic rates of ferns and gymnosperms as compared to angiosperms, since we show that they have greater mesophyll volume per stoma, acting as a bottleneck that limits their evaporative capacities (Supplementary Fig. 5).

Current increases in temperature and atmospheric CO_2 concentrations might impact the structure and function of conifer forests worldwide, and it has been posed that improved WUE could alleviate the temperature effect [7]. Previous studies have shown higher WUE_i under increasing CO_2 in conifer species, having stronger WUE_i responses than angiosperms [44-46]. Additionally, it has been recently shown that higher plasticity in the vascular tissue of the needles of *Pinus pinaster* enhances WUE_i [47]. Using an experimental approach, needles of *Larix kaempferi* growing under higher CO_2 and nutrient supplies showed increased mesophyll surface area per leaf area, coupled with higher photosynthetic rates[48]. Moreover, it was shown that elevated CO_2 increased mesophyll surface and decreased stomatal density in *Pinus sylvestris* needles [49]. Therefore, under such elevated CO_2 conditions, we might expect to observe a lower stomata/V_{mes} ratio, which would enhance WUE_i according to our predictions (Fig. 5b). Covariation and coordinated changes in vascular and mesophyll tissue volumetrics, along with stomatal pore number in conifer leaves, may allow conifer species to cope and adapt to the pressure exerted by increasing VPD by maintaining similar carbon assimilation levels with lower water consumption.

Materials and Methods

Plant material. Sampling included 34 conifer species representing species from various biomes, physiologies, and leaf shapes. Sampling included taxa from four different families of conifers: Araucariaceae (2 spp), Pinaceae (30 spp), Podocarpaceae (1sp), and Taxaceae (1 sp). Our sampling particularly focused on the genus *Pinus* with 26 species including representatives from the two subgenera *Pinus* (21 spp) and *Strobus* (5 spp), which differ in the number of vascular bundles per leaf [35]. Fully expanded leaves from adult plants were collected in the Berkeley Arboretum of the University of California Botanical Garden, and the University of Georgia's Thompson Mills Arboretum. Samples from both locations were used for microCT scanning and gas exchange measurements. Whole shoots were cut, wrapped in moist paper towels, and transported in dark plastic bags to avoid desiccation before scanning.

X-ray microtomography (microCT) scanning and image segmentation. MicroCT imaging was performed at the Lawrence Berkeley National Laboratory Advanced Light Source, beamline 8.3.2. Leaves were scanned within 24h of excision. Samples were wrapped with a polyimide (Kapton) tape, which allows x-ray transmittance while preventing sample desiccation. Wrapped leaf samples were placed in a plastic 1000 µL pipette tip with the lower end submerged in water and centered in the microCT x-ray beam. Scans were completed in c. 15 minutes in continuous tomography mode at 21 keV capturing 1,025 projection images of XYZ ms each. Images were captured using alternatively 5x or 10x objective lenses depending on leaf diameter, yielding final pixel resolutions of 1.27 µm and 0.625 µm. Images were reconstructed using TomoPy [50]. Raw tomographic datasets were reconstructed using both gridrec and phase retrieval methods, both of which yield complementary results being efficient in segmenting cell boundaries and larger air voids, respectively [26]. Image stacks of c. 2600 8-bit grayscale images were generated from the reconstruction process. Airspace was segmented in both gridrec and phase reconstruction methods by visually defining a range of pixel intensity values and the binary image stacks from both reconstruction methods were combined. Boundaries delimiting the areas occupied by the bundle sheath + transfusion tissue, epidermis, mesophyll, resin ducts, and veins were manually drawn using a graphic tablet (Wacom Cintiq Pro 16, Wacom Co, Saitama, Japan) in ImageJ [51]. Leaf veins were depicted here as the vascular bundle comprising both xylem and phloem tissues. Leaf tissue boundaries were drawn as regions of interest (ROIs) in six to eight images randomly distributed across the full stack. The combination of the binary image derived from both reconstruction methods, along with the tissue boundaries, resulted in a composite image stack where each

leaf tissue was classified. Leaf segmentation, which allowed us to automatically delimit different tissues across the full stack using a limited set of hand-segmented composite slices was done using random-forest classification [52; https://github.com/plant-microct-tools/leaf-traits-microct].

Three-dimensional anatomy and stomatal traits. We extracted the volume and surface area of leaf anatomical traits from the full segmented stacks [52]. We estimated the volumes of the epidermis (V_{ep}), bundle sheath and transfusion tissue (V_{BS+TT}), mesophyll cells (V_{cell}), mesophyll intercellular airspace (V_{IAS}), resin ducts (V_{resin}), and veins (V_{vein}). Mesophyll volume (V_{mes}) was estimated as the sum of V_{cell} and V_{IAS}. All volume metrics are reported in μm^3. Relative volumes for each tissue (in $\mu m^3\ \mu m^{-3}$) were estimated as a fraction of tissue per V_{leaf}, total leaf volume. We calculated mesophyll porosity ($\mu m^3\ \mu m^{-3}$) as V_{IAS}/V_{mes}. The mesophyll surface area exposed to the intercellular airspace (SA_{mes}) was used to estimate the mesophyll surface area per mesophyll volume (SA_{mes}/V_{mes}; $\mu m^2\ \mu m^{-3}$). Additionally, we estimated the exposed mesophyll surface area per bundle sheath volume (SA_{mes}/V_{BS+TT}; $\mu m^2\ \mu m^{-3}$) and vein volume (SA_{mes}/V_{vein}; $\mu m^2\ \mu m^{-3}$). Leaf area A_{leaf} (μm^2) was measured by summing up the perimeter of each slice and multiplying it by slice depth. We used the ratio SA_{mes}/A_{leaf} to calculate the mesophyll surface area per total leaf area (S_m; $\mu m^2\ \mu m^{-2}$). Stomatal estimations were performed by counting all visible stomata on the leaf surface of each scan using Avizo 9.4 software (FEI Co. Hillsboro, OR, USA). Absolute stomatal counts were used in relation to mesophyll volumetric anatomy to estimate traits accounting for the interaction of stomata pore number and V_{IAS}, V_{mes}, and SA_{mes} units. Mesophyll volumetric features were assessed in mm^3 for stomatal pore density estimations. We also accounted for stomatal number per leaf surface to assess potential differences in stomatal density estimations based on surface vs volume fractions. Further, we performed a comparison of surface- and volume-based anatomical estimations using 2D slices and the full 3D stack (Supplementary Fig. 3). Methods are further explained in the Supplementary Text 1. Average trait values for each species are available in Supplementary Dataset 1 (available on request). A list of measured anatomical variables, including abbreviations and units, is available in Supplementary Table 1.

Gas exchange and water use efficiency measurements. Maximum stomatal conductance (g_{smax}; mmol $m^{-2}\ s^{-1}$) and light-saturated CO_2 assimilation rate (A_{sat}; µmol $m^{-2}\ s^{-1}$) were measured with a LICOR-6800 gas exchange system (LI-COR biosciences, Lincoln, NE, USA) between 9:00 and 14:00 on fully sunlit outer canopy foliage. Chamber temperature was

set to 25° C, light source was set to 1500 µmol m^{-2} s^{-1} and chamber CO_2 was set to 400 ppm. Following the gas exchange measurements, the leaf area contained within the chamber was marked using a permanent marker, collected, and the projected leaf area was measured using a leaf area meter (LI3100C, LI-COR biosciences, Lincoln, NE, USA). A_{sat} and g_{smax} were estimated on a subset of 18 species (Supplementary Dataset 1, available on request) and used to estimate leaf-level intrinsic water use efficiency ($WUE_i = A_{sat}/g_{smax}$; µmol mol^{-1}). *Pinus strobus* A_{sat} data was removed prior to analyses due to potential measurement inaccuracies.

Data analysis. All statistical analyses and data treatment were performed using R v.3.6.3 [53]. Anatomical traits were assembled and averaged for each species for data analysis. Assumptions for residual homogeneity and normality were tested prior to data analyses. Phylogenetic relationships, including branch length calibrations and divergence times, were obtained from published data [54,55]. To predict leaf physiological traits based on volumetric anatomical variables we used phylogenetic generalized least-squares analyses (PGLS) with a lambda (λ) maximum likelihood optimization to control for phylogenetic non-independence between related species [56,57]. The assemblage of the composite phylogenetic tree of studied conifers (Supplementary Dataset 3, available on request) was carried out using the package 'ape' [58] and PGLS models were fit using the package 'caper' [59]. Standard major axis (SMA) were implemented with the package 'smatr' [60] to test allometric scaling between tissue volumes. A principal component analysis (PCA) was used to explore the covariation of selected traits and the distribution of conifer groups as explained by the physiological and anatomical traits measured. Given the marked differences in leaf anatomical structure between *Pinus* subgenera *Pinus* and *Strobus*, we explored potential variation in 3D anatomical traits by plotting each group within the PCA. We further explored differences between these clades by performing a one-way ANOVA on measured structural traits. A similar variance meta-analysis, including post hoc Tukey's honest significant differences, was employed to compare the studied conifer species with other gymnosperms, along with angiosperms and ferns. Data for comparisons across plant groups was obtained from a recently published study Supplementary Dataset 2 [23] (available on request).

References

1 de Boer, H. J., Eppinga, M. B., Wassen, M. J. & Dekker, S. C. A critical transition in leaf evolution facilitated the Cretaceous angiosperm revolution. *Nature Communications* **3**, 1221 (2012).

2 Boyce, C. K., Brodribb, T. J., Feild, T. S. & Zwieniecki, M. A. Angiosperm leaf vein evolution was physiologically and environmentally transformative. *Proceedings of the Royal Society B: Biological Sciences* **276**, 1771-1776 (2009).

3 Crepet, W. L. & Niklas, K. J. Darwin's second "abominable mystery": Why are there so many angiosperm species? *American Journal of Botany* **96**, 366-381 (2009).

4 Bond, W. J. The tortoise and the hare: ecology of angiosperm dominance and gymnosperm persistence. *Biological Journal of the Linnean Society* **36**, 227-249 (1989).

5 Brodribb, T. J., Pittermann, J. & Coomes, D. A. Elegance versus Speed: Examining the Competition between Conifer and Angiosperm Trees. *International Journal of Plant Sciences* **173**, 673-694 (2012).

6 McFarlane, P. & Sands, R. Wood and paper products. *Forestry in a global context*, 77-97 (2013).

7 Brodribb, T. J., Powers, J., Cochard, H. & Choat, B. Hanging by a thread? Forests and drought. *Science* **368**, 261 (2020).

8 Dai, A. Drought under global warming: a review. *Wiley Interdisciplinary Reviews: Climate Change* **2**, 45-65 (2011).

9 Kharuk, V. I. *et al.* Climate-driven conifer mortality in Siberia. *Global Ecology and Biogeography* **30**, 543-556 (2021).

10 Blackmore, S., Gibby, M. & Rae, D. Strengthening the scientific contribution of botanic gardens to the second phase of the Global Strategy for Plant Conservation. *Botanical Journal of the Linnean Society* **166**, 267-281 (2011).

11 Grossiord, C. *et al.* Plant responses to rising vapor pressure deficit. *New Phytologist* **226**, 1550-1566 (2020).

12 Choat, B. *et al.* Triggers of tree mortality under drought. *Nature* **558**, 531-539 (2018).

13 Keenan, T. F. *et al.* Increase in forest water-use efficiency as atmospheric carbon dioxide concentrations rise. *Nature* **499**, 324-327 (2013).

14 Mathias, J. M. & Thomas, R. B. Global tree intrinsic water use efficiency is enhanced by increased atmospheric CO_2 and modulated by climate and plant functional types. *Proceedings of the National Academy of Sciences* **118**, e2014286118 (2021).

15 Guerrieri, R. *et al.* Disentangling the role of photosynthesis and stomatal conductance on rising forest water-use efficiency. *Proceedings of the National Academy of Sciences* **116**, 16909 (2019).

16 Hetherington, A. M. & Woodward, F. I. The role of stomata in sensing and driving environmental change. *Nature* **424**, 901-908 (2003).

17 Flexas, J. *et al.* Mesophyll diffusion conductance to CO2: An unappreciated central player in photosynthesis. *Plant Science* **193-194**, 70-84 (2012).

18 Gago, J. *et al.* Mesophyll conductance: the leaf corridors for photosynthesis. *Biochemical Society Transactions* **48**, 429-439 (2020).

19 Carriquí, M. *et al.* Cell wall composition strongly influences mesophyll conductance in gymnosperms. *The Plant Journal* **103**, 1372-1385 (2020).

20 Nobel, P. S., Zaragoza, L. J. & Smith, W. K. Relation between Mesophyll Surface Area, Photosynthetic Rate, and Illumination Level during Development for Leaves of *Plectranthus parviflorus* Henckel. *Plant Physiology* **55**, 1067 (1975).

21 Smith, W. K. & Nobel, P. S. Influences of Seasonal Changes in Leaf Morphology on Water-Use Efficiency For Three Desert Broadleaf Shrubs. *Ecology* **58**, 1033-1043 (1977).

22 Earles, J. M. *et al.* Beyond porosity: 3D leaf intercellular airspace traits that impact mesophyll conductance. *Plant Physiology* (2018).

23 Théroux-Rancourt, G. *et al.* Maximum CO2 diffusion inside leaves is limited by the scaling of cell size and genome size. *Proceedings of the Royal Society B: Biological Sciences* **288**, 20203145 (2021).

24 Lundgren, M. R. *et al.* Mesophyll porosity is modulated by the presence of functional stomata. *Nature Communications* **10**, 2825 (2019).

25 Evans, J. R., Kaldenhoff, R., Genty, B. & Terashima, I. Resistances along the CO2 diffusion pathway inside leaves. *Journal of Experimental Botany* **60**, 2235-2248 (2009).

26 Théroux-Rancourt, G. *et al.* The bias of a two-dimensional view: comparing two-dimensional and three-dimensional mesophyll surface area estimates using noninvasive imaging. *New Phytologist* **215**, 1609-1622 (2017).

27 Earles, J. M. *et al.* Embracing 3D Complexity in Leaf Carbon–Water Exchange. *Trends in Plant Science* **24**, 15-24 (2019).

28 Zwieniecki, M. A., Boyce, C. K. & Holbrook, N. M. Functional Design Space of Single-veined Leaves: Role of Tissue Hydraulic Properties in Constraining Leaf Size and Shape. *Annals of Botany* **94**, 507-513 (2004).

29 Brodribb, T. J., Feild, T. S. & Sack, L. Viewing leaf structure and evolution from a hydraulic perspective. *Functional Plant Biology* **37**, 488-498 (2010).

30 Brodribb, T. J. & Feild, T. S. Stem hydraulic supply is linked to leaf photosynthetic capacity: evidence from New Caledonian and Tasmanian rainforests. *Plant, Cell & Environment* **23**, 1381-1388 (2000).

31 Hu, Y.-S. & Yao, B.-J. Transfusion tissue in gymnosperm leaves. *Botanical Journal of the Linnean Society* **83**, 263-272 (1981).

32 Breshears, D. D. *et al.* A Dirty Dozen Ways to Die: Metrics and Modifiers of Mortality Driven by Drought and Warming for a Tree Species. *Frontiers in Forests and Global Change* **1** (2018).

33 Gaylord, M. L. *et al.* Drought predisposes piñon–juniper woodlands to insect attacks and mortality. *New Phytologist* **198**, 567-578 (2013).

34 Brodribb, T. J., McAdam, S. A. M., Jordan, G. J. & Martins, S. C. V. Conifer species adapt to low-rainfall climates by following one of two divergent pathways. *Proceedings of the National Academy of Sciences* **111**, 14489-14493 (2014).

35 Gernandt, D. S., López, G. G., García, S. O. & Liston, A. Phylogeny and classification of Pinus. *TAXON* **54**, 29-42 (2005).

36 Martínez-Vilalta, J., Sala, A. & Piñol, J. The hydraulic architecture of Pinaceae – a review. *Plant Ecology* **171**, 3-13 (2004).

37 Zwieniecki, M. A., Brodribb, T. J. & Holbrook, N. M. Hydraulic design of leaves: insights from rehydration kinetics. *Plant, Cell & Environment* **30**, 910-921 (2007).

38 Carins Murphy, M. R., Jordan, G. J. & Brodribb, T. J. Acclimation to humidity modifies the link between leaf size and the density of veins and stomata. *Plant, Cell & Environment* **37**, 124-131 (2014).

39 Brodribb, T. J. & Feild, T. S. Evolutionary significance of a flat-leaved Pinus in Vietnamese rainforest. *New Phytologist* **178**, 201-209 (2008).

40 Brodribb, T. J., Feild, T. S. & Jordan, G. J. Leaf Maximum Photosynthetic Rate and Venation Are Linked by Hydraulics. *Plant Physiology* **144**, 1890-1898 (2007).

41 Johnson, D. M., Smith, W. K., Vogelmann, T. C. & Brodersen, C. R. Leaf architecture and direction of incident light influence mesophyll fluorescence profiles. *American Journal of Botany* **92**, 1425-1431 (2005).

42 Esau, K. *Anatomy of seed plants (2nd edn)*. (1977).

43 Mediavilla, S., Escudero, A. & Heilmeier, H. Internal leaf anatomy and photosynthetic resource-use efficiency: interspecific and intraspecific comparisons. *Tree Physiology* **21**, 251-259 (2001).

44 Dalling, J. W. *et al.* Two tropical conifers show strong growth and water-use efficiency responses to altered CO2 concentration. *Annals of Botany* **118**, 1113-1125 (2016).

45 Klein, T. *et al.* Growth and carbon relations of mature Picea abies trees under 5 years of free-air CO2 enrichment. *Journal of Ecology* **104**, 1720-1733 (2016).

46 Adams, M. A., Buckley, T. N. & Turnbull, T. L. Diminishing CO2-driven gains in water-use efficiency of global forests. *Nature Climate Change* **10**, 466-471 (2020).

47 Bert, D., Le Provost, G., Delzon, S., Plomion, C. & Gion, J. M. Higher needle anatomic plasticity is related to better water-use efficiency and higher resistance to embolism in fast-growing Pinus pinaster families under water scarcity. *Trees* **35**, 287-306 (2021).

48 Eguchi, N. *et al.* Changes in Morphology, Anatomy, and Photosynthetic Capacity of Needles of Japanese Larch (Larix kaempferi) Seedlings Grown in High CO2 Concentrations. *Photosynthetica* **42**, 173-178 (2004).

49 Lin, J., Jach, M. E. & Ceulemans, R. Stomatal density and needle anatomy of Scots pine (Pinus sylvestris) are affected by elevated CO2. *New Phytologist* **150**, 665-674 (2001).

50 Gürsoy, D., De Carlo, F., Xiao, X. & Jacobsen, C. TomoPy: a framework for the analysis of synchrotron tomographic data. *Journal of synchrotron radiation* **21**, 1188-1193 (2014).

51 Schneider, C. A., Rasband, W. S. & Eliceiri, K. W. NIH Image to ImageJ: 25 years of image analysis. *Nat Methods* **9**, 671-675 (2012).

52 Théroux-Rancourt, G. *et al.* Digitally deconstructing leaves in 3D using X-ray microcomputed tomography and machine learning. *Applications in Plant Sciences* **8**, e11380 (2020).

53 R: A language and environment for statistical computing. Vienna, Austria: R Foundation for Statistical Computing (2020).

54 Smith, S. A. & Brown, J. W. Constructing a broadly inclusive seed plant phylogeny. *American Journal of Botany* **105**, 302-314 (2018).

55 Magallón, S., Gómez-Acevedo, S., Sánchez-Reyes, L. L. & Hernández-Hernández, T. A metacalibrated time-tree documents the early rise of flowering plant phylogenetic diversity. *New Phytologist* **207**, 437-453 (2015).

56 Felsenstein, J. Phylogenies and the Comparative Method. *The American Naturalist* **125**, 1-15 (1985).

57 Freckleton, R. P., Harvey, P. H. & Pagel, M. Phylogenetic analysis and comparative data: a test and review of evidence. *The American Naturalist* **160**, 712-726 (2002).

58 Paradis, E. & Schliep, K. ape 5.0: an environment for modern phylogenetics and evolutionary analyses in R. *Bioinformatics* **1**, 3 (2018).

59 Orme, D. *et al.* caper: comparative analyses of phylogenetics and evolution in R, R package version 1.0. 1. (2018).

60 Warton, D. I., Duursma, R. A., Falster, D. S. & Taskinen, S. smatr 3– an R package for estimation and inference about allometric lines. *Methods in Ecology and Evolution* **3**, 257-259 (2012).

Acknowledgments

This work was supported by the NSF grants IOS-1626966, IOS-1852976 and IOS-1146746, the Austrian Science Fund (FWF), project M2245, and the Vienna Science and Technology Fund (WWTF), project LS19-013. We thank the Berkeley Arboretum of the University of California Botanical Garden, and the University of Georgia's Thompson Mills Arboretum for providing plant material. The Advanced Light Source is supported by the Director, Office of Science, Office of Basic Energy Science, of the U.S. Department of Energy under contract no. DE-AC02-05CH11231. TNB acknowledges support from the USDA National Institute of Food and Agriculture (Hatch Award 1016439 and Award 2020-67013-30913) and the NSF (IOS-1951244, IOS-1557906)

Supplementary Information – Preprint Version

The 3D construction of leaves is coordinated with water use efficiency in conifers.

Santiago Trueba[1,2,*], Guillaume Théroux-Rancourt[3], J Mason Earles[4], Thomas N. Buckley[5], David Love[6], Daniel M Johnson[6], Craig Brodersen[1].

[1] *School of the Environment, Yale University, New Haven, CT, USA.*
[2] *University of Bordeaux, INRAE, BIOGECO, Pessac, France.*
[3] *Institute of Botany, University of Life Sciences and Natural Resources, Vienna, Austria.*
[4] *Department of Viticulture and Enology, University of California Davis, CA, USA.*
[5] *Department of Plant Sciences, University of California Davis, CA, USA.*
[6] *Warnell School of Forestry and Natural Resources, University of Georgia, GA, USA.*

[*]Corresponding author: strueba@gmail.com

Supplementary Information includes:

Supplementary text S1.

Supplementary Figures 1 to 5.

Supplementary Tables 1 to 4.

Other supplementary materials available upon request:

Supplementary Datasets 1 to 3.

Supplementary Text 1. Since methods to generate volumetric anatomical data are less available, we were interested in providing a robust alternative using anatomical cross sections, which can be produced using standard microscopy protocols. Our study shows that V_{vein}/V_{leaf}, the ratio of vein volume over leaf volume, is a powerful explanatory variable, accurately predicting intrinsic water use efficiency (WUE_i) in conifers (see main text). Given that conifer leaves have a rather homogenous anatomy along their length, we expected that the V_{vein}/V_{leaf} ratio would be strongly related to the vein surface over leaf surface ratio (A_{vein}/A_{leaf}), which can be measured using standard light microscopy methods on needle cross sections, for example. To test this assumption, we programmatically measured A_{vein}/A_{leaf} on all slices of each of our scanned and segmented conifer leaf stacks (34 species; total number of slices between ~200 and 2000) and computed the median value as well as the standard deviation. The relationship between the whole stack median A_{vein}/A_{leaf} and V_{vein}/V_{leaf} was very strong ($A_{vein}/A_{leaf} = 0.0005 + 0.9923\ V_{vein}/V_{leaf}$; $R^2 = 0.98$, $p < 0.0001$). However, we wanted to know if we can reach a similar relationship using the common practice of average anatomical data over a few sections. To do so, we sample one to 50 different slices from the whole stack data, computed the mean A_{vein}/A_{leaf} from that sample, and repeated that 30 times for each number of slice and for each image stack (Supplementary Figure S4 present data for one to six pooled slices). Using only one slice to estimate A_{vein}/A_{leaf} give substantially more bias compared to the actual V_{vein}/V_{leaf} measured, with a larger range of possible values even if the median is close to a 1:1 relationship ($A_{vein}/A_{leaf} = 0.0010 + 0.9576\ V_{vein}/V_{leaf}$; $R^2 = 0.86$, $p < 0.0001$). Using the mean of three slices produces A_{vein}/A_{leaf} more comparable to V_{vein}/V_{leaf}, and where 95% of the data falls within one standard deviation of the whole stack A_{vein}/A_{leaf} data ($A_{vein}/A_{leaf} = 0.0008 + 0.9728\ V_{vein}/V_{leaf}$; $R^2 = 0.95$, $p < 0.0001$). Averaging over more slices would increase the strength of the relationship. Thus, our analysis shows that area ratios could be used instead of volumetric data. However, as volumetric data provides information over a substantially larger portion of a leaf compared to a few cross sections, it will always provide more accurate data, even in anatomically homogenous leaves such as those of conifer species.

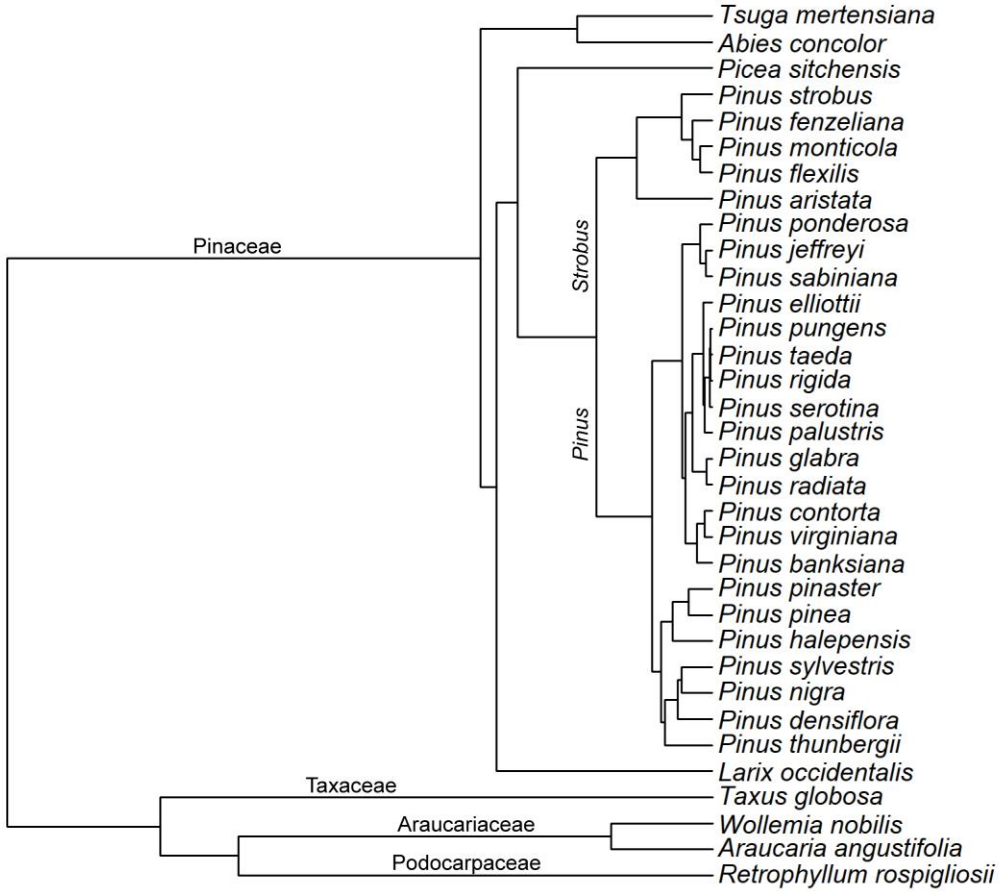

Supplementary Figure 1. Phylogenetic relationships across the 34 studied species. Labels in branches correspond to different conifer families (horizontal) and *Pinus* subgenera (vertical). The file containing the phylogenetic tree is available as supplementary information (Dataset S3).

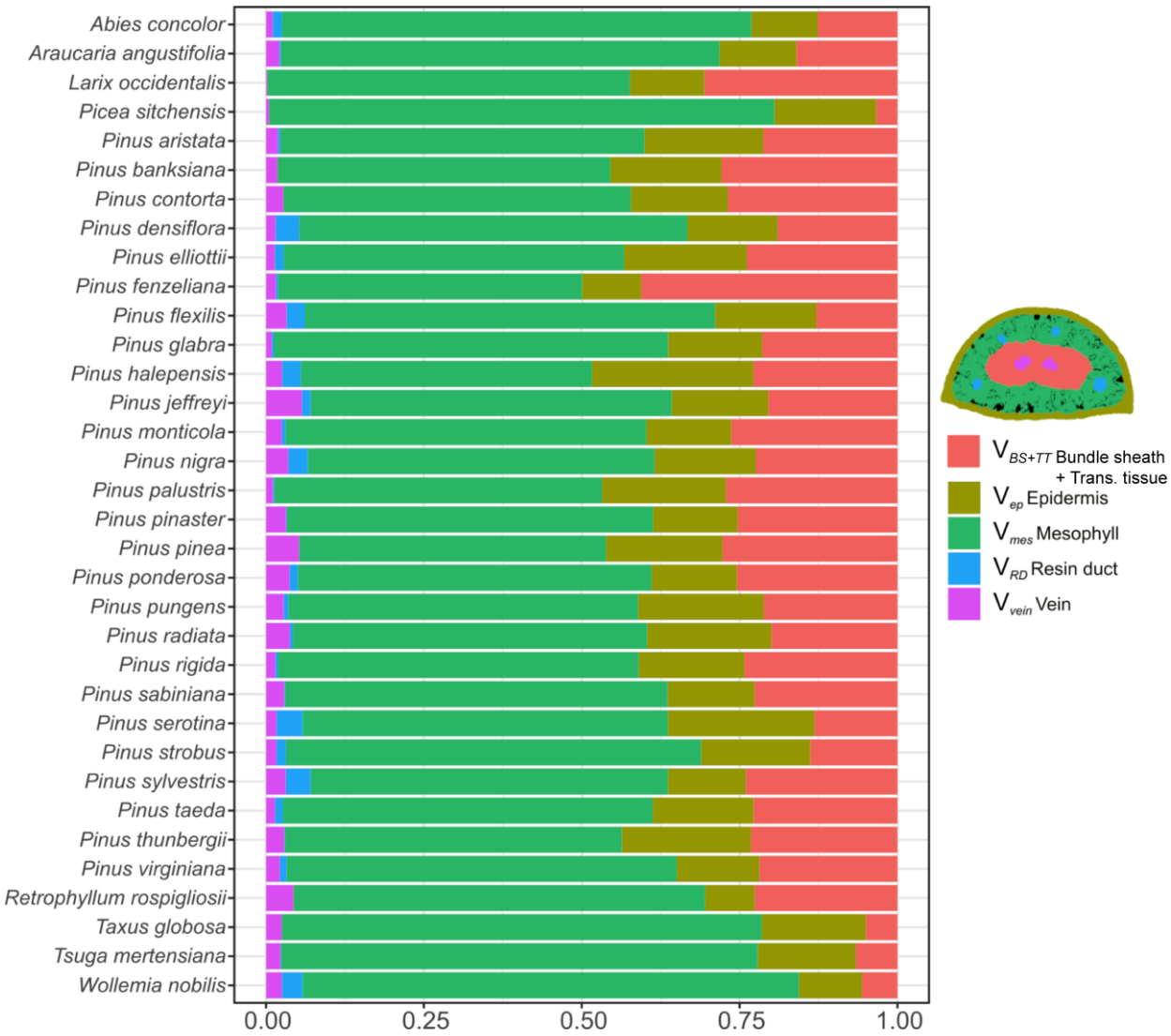

Supplementary Figure 2. Proportion of tissue relative volumes inside the 3D leaf space for the 34 conifer species studied.

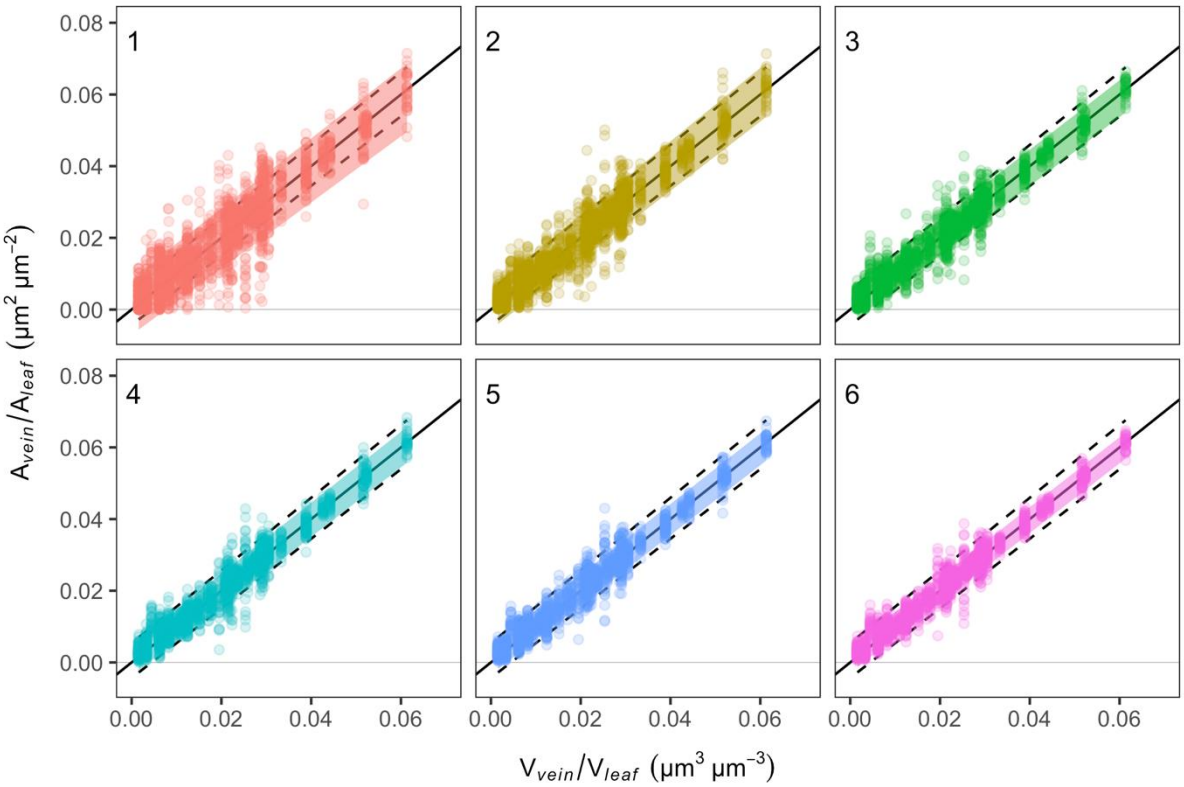

Supplementary Figure 3. Relationship between vein volume over leaf volume ratio (V_{vein}/V_{leaf}), measured over the whole image stack, and the vein area over leaf area ratio (A_{vein}/A_{leaf}), measured on single image slices of the stacks. In each panel, points represent the mean value of A_{vein}/A_{leaf} for one to six slices sampled from data collected on each slices of the stack (numbers upper left of the panels represent the number of slices averaged over). Colored ribbons represent the region where 95% of the data lie, and dotted lines represent the A_{vein}/A_{leaf} median ± standard deviation for the whole stack (measured from ~200-2000 slices depending on the stack). See the Supplementary Text S1 for additional details.

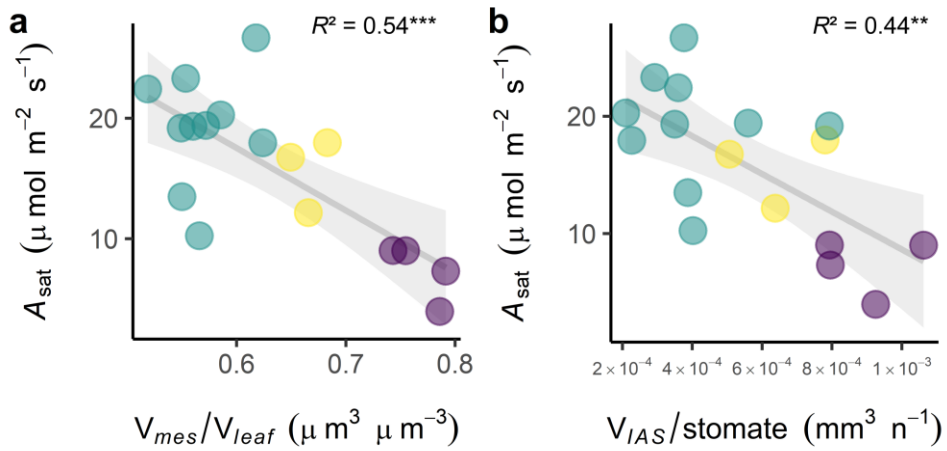

Supplementary Figure 4. Light-saturated photosynthetic assimilation (A_{sat}) as a function of volumetric anatomy and stomatal traits in conifers. Relationships of A_{sat} with relative mesophyll volume (a) and inter-cellular air space volume (IAS) per stomatal number (b). Solid regression lines and 95% confidence intervals are included. *Pinus* species from the subgenera *Pinus* (green circles) and *Strobus* (yellow circles), along with other conifer species (purple circles) are indicated. PGLS coefficients of determination are included. ** $p < 0.01$; *** $p < 0.001$. Additional information available in Supplementary Table 4.

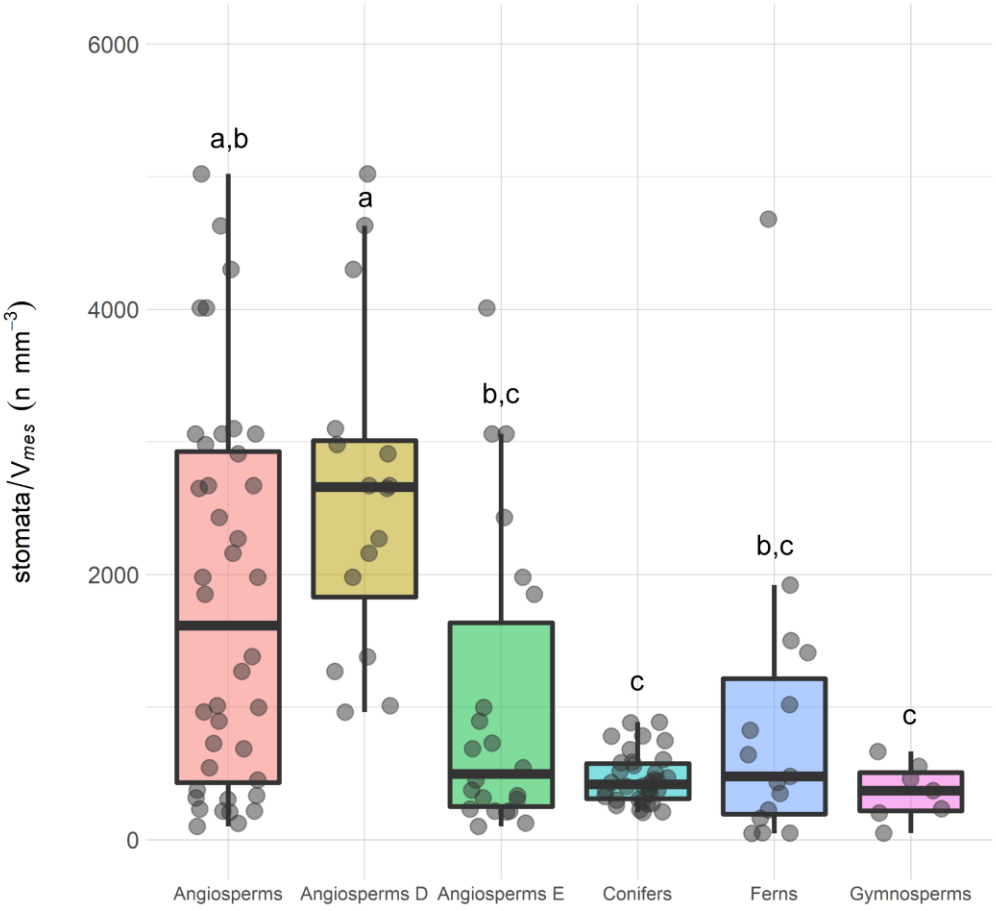

Supplementary Figure 5. Stomatal number per mesophyll volume across different plant groups. Conifer species measured in this study (34 spp) are compared with published data (1) for other gymnosperms (7 spp) angiosperms (39 spp) and ferns (16 spp). A distinction between deciduous (D; 17 spp) and evergreen (E; 22 spp) angiosperm species is also included. Significant differences after a one-way analysis of variance followed by a post hoc Tukey's honest significance differences using 95% confidence intervals are indicated with different letters. The dataset is included as supplementary material (Dataset S2).

Supplementary Table 1. Abbreviations and definitions of anatomical and gas exchange variables measured, with reference to their units.

Abbreviation	Definition	Units
A_{sat}	Light-saturated photosynthetic assimilation rate	µmol m^{-2} s^{-1}
g_{smax}	Maximum stomatal conductance	mmol m^{-2} s^{-1}
Porosity	Mesophyll porosity	µm^3 µm^{-3}
SA_{mes}/**stomate**	Mesophyll surface area per stomate	mm^2 n^{-1}
SA_{mes}/V_{BS+TT}	Mesophyll surface area per unit bundle sheath and transfusion tissue volume	µm^2 µm^{-3}
SA_{mes}/V_{mes}	Mesophyll surface area per unit mesophyll volume	µm^2 µm^{-3}
SA_{mes}/V_{vein}	Mesophyll surface area per unit vein volume	µm^2 µm^{-3}
S_m	Mesophyll surface area per total leaf area	µm^2 µm^{-2}
stomata/A_{leaf}	Stomatal pore number per unit leaf area	n mm^{-2}
stomata/SA_{mes}	Stomatal pore number per unit mesophyll surface area	n mm^{-2}
stomata/V_{IAS}	Stomatal pore number per unit mesophyll intercellular airspace volume	n mm^{-3}
stomata/V_{mes}	Stomatal pore number per unit mesophyll volume	n mm^{-3}
V_{BS+TT}/V_{leaf}	Bundle sheath and transfusion tissue volume relative to total leaf volume	µm^3 µm^{-3}
V_{ep}/V_{leaf}	Epidermis volume relative to total leaf volume	µm^3 µm^{-3}
V_{IAS}/**stomate**	Intercellular airspace volume per stomate	mm^3 n^{-1}
V_{mes}/**stomate**	Mesophyll volume per stomate	mm^3 n^{-1}
V_{mes}/V_{leaf}	Mesophyll volume relative to total leaf volume	µm^3 µm^{-3}
V_{resin}/V_{leaf}	Resin duct volume relative to total leaf volume	µm^3 µm^{-3}
V_{vein}/V_{leaf}	Vein volume relative to total leaf volume	µm^3 µm^{-3}
WUE_i	Intrinsic water use efficiency	µmol mol^{-1}

Supplementary Table 2. Structural coordination within the volumetric space of the conifer leaf. Standardized major axis (SMA) matrix across volumetric anatomical traits in conifer leaves showing r^2 (above diagonal) and *p*-values (below diagonal). Significant relations at α = 0.05 are indicated.

	Porosity	**V_{mes}/V_{leaf}**	**V_{vein}/V_{leaf}**	**V_{BS+TT}/V_{leaf}**	**V_{resin}/V_{leaf}**	**V_{ep}/V_{leaf}**	**stomata/V_{mes}**	**stomata/SA_{mes}**	**SA_{mes}/V_{mes}**	**SA_{mes}/V_{vein}**	**S_m**
Porosity		**0.41**	0.06	0.01	0	0.07	0.09	0.05	0.03	**0.17**	0.02
V_{mes}/V_{leaf}	**<0.001**		0.1	0.07	0.03	**0.27**	**0.19**	0.08	0.04	**0.17**	0
V_{vein}/V_{leaf}	0.15	0.07		0	0	0.01	0.08	**0.12**	0.02	**0.37**	**0.15**
V_{BS+TT}/V_{leaf}	0.66	0.12	0.72		0.05	0	0	0.01	0.05	0	**0.16**
V_{resin}/V_{leaf}	0.87	0.33	0.90	0.19		0	0.02	0	0.04	0.03	0.01
V_{ep}/V_{leaf}	0.13	**<0.01**	0.52	0.84	0.93		0.02	0	0.02	0	0.03
stomata/V_{mes}	0.09	**<0.01**	0.10	0.95	0.47	0.39		**0.75**	0.01	0	0.04
stomata/SA_{mes}	0.21	0.10	**<0.05**	0.55	0.87	0.80	**<0.001**		**0.13**	0.01	**0.27**
SA_{mes}/V_{mes}	0.35	0.25	0.40	0.19	0.25	0.39	0.52	**<0.05**		0	**0.5**
SA_{mes}/V_{vein}	**<0.05**	**<0.05**	**<0.001**	0.76	0.35	0.79	0.77	0.68	0.99		0.01
S_m	0.46	0.71	**<0.05**	**<0.05**	0.66	0.34	0.24	**<0.01**	**<0.001**	0.52	

Supplementary Table 3. Comparisons of volumetric anatomy between *Pinus* subgenera *Pinus* and *Strobus*, and other conifer species. Average values for each conifer group are included. Significant differences detected with a one-way ANOVA followed by post hoc Tukey's honest significance differences tests are indicated with different letters. Significant differences between conifer groups at α = 0.05 are also indicated in bold. Graphic representations of some focal comparisons are presented in Fig. S3. *Physiological data measured on a subset of 18 species, different degrees of freedom (2,15) apply to these specific comparisons.

Trait	*Pinus*	*Strobus*	Other conifers	Sum of squares	Mean square	*F* value (2,31)	Significance
Porosity	0.20^{b}	$0.24^{a,b}$	0.28^{a}	0.03438	0.017191	11.75	**0.00016**
SA_{mes}/stomate	267004^{b}	$290208^{a,b}$	414000^{a}	1.265e+11	6.323e+10	3.766	**0.034**
SA_{mes}/V_{BS+TT}	0.32^{b}	0.46^{b}	1.28^{a}	5.447	9.911	2.7237	**0.00047**
SA_{mes}/V_{mes}	0.13^{a}	0.12^{a}	0.12^{a}	0.000502	0.0002512	0.257	0.77
SA_{mes}/V_{vein}	3.49^{a}	$4.55^{a,b}$	10.37^{b}	277.9	138.93	3.862	**0.032**
S_m	11.26^{a}	9.15^{a}	12.62^{a}	37.1	18.57	0.882	0.42
stomata/SA_{mes}	$4.40e\text{-}6^{a}$	$3.66e\text{-}6^{a,b}$	$2.88e\text{-}6^{b}$	1.377e-11	6.884e-12	3.312	**0.050**
stomata/V_{IAS}	$2.72e\text{-}6^{a}$	$1.75e\text{-}6^{a,b}$	$1.15e\text{-}6^{b}$	1.546e-11	7.73e-12	10	**0.00044**
stomata/V_{mes}	$5.34e\text{-}7^{a}$	$4.32e\text{-}7^{a,b}$	$3.12e\text{-}7^{b}$	2.938e-13	1.469e-13	5.394	**0.0098**
V_{BS+TT}/V_{leaf}	$0.23^{a,b}$	0.28^{b}	0.14^{b}	0.06877	0.03438	3.911	**0.031**
V_{ep}/V_{leaf}	0.17^{a}	0.17^{a}	$0.13^{a,b}$	0.00829	0.004147	3.995	**0.029**
V_{mes}/V_{leaf}	0.55^{a}	0.67^{b}	0.75^{c}	0.24492	0.12246	70.59	**2.88e-12**
V_{resin}/V_{leaf}	0.01^{a}	0.01^{a}	0.006^{a}	0.000218	0.0001088	0.653	0.528
V_{vein}/V_{leaf}	0.03^{a}	0.02^{a}	0.02^{a}	0.000245	0.0001224	0.807	0.456
V_{IAS}/stomate	441464^{b}	605340^{b}	948887^{a}	1.494e+12	7.470e+11	18.05	**6.33e-06**
V_{mes}/stomate	2143982^{b}	$2587971^{a,b}$	3496859^{a}	1.062e+13	5.312e+12	7.061	**0.0030**
A_{sat}*	19.22^{a}	21.91^{a}	7.32^{b}	520.1	260.03	5.50	**0.016**
g_{smax}*	0.20^{a}	0.19^{a}	0.07^{a}	0.05194	0.025971	2.713	0.099
WUE_i*	105.89^{a}	122.51^{a}	115.94^{a}	877	438.3	0.632	0.54

Supplementary Table 4. Variation in gas exchange, photosynthesis and water use efficiency as explained by leaf volumetric anatomy and stomatal traits. Phylogenetic generalized least squares (PGLS) statistics are included and significant relations at α = 0.05 are indicated.

	A_{sat}					g_{smax}					WUE_i				
	Intercept	Slope	R^2	*P*-value	λ	Intercept	Slope	R^2	*P*-value	λ	Intercept	Slope	R^2	*P*-value	λ
Porosity	**32.35**	**-79.45**	**0.39**	**<0.01**	**0.00**	0.23	-0.29	0.02	0.58	0.00	93.61	85.66	0.03	0.50	0.00
$SA_{mes/}$ stom	12.65	-8.88e-6	0.07	0.31	0.75	**0.28**	**-3.31e-7**	**0.27**	**<0.05**	**0.00**	**95.96**	**8.68e-5**	**0.26**	**<0.05**	**0.67**
SA_{mes}/V_{BS+TT}	**15.66**	**-5.92**	**0.28**	**<0.05**	**0.53**	0.21	-0.07	0.16	0.10	0.00	113.97	-3.22	0.01	0.75	0.00
SA_{mes}/V_{mes}	13.95	-43.53	0.05	0.36	0.84	0.22	-0.40	0.01	0.70	0.00	96.06	125.52	0.02	0.61	0.00
SA_{mes}/V_{vein}	11.56	-0.36	0.07	0.32	0.74	0.02	0.01	0.20	0.06	0.79	**144.83**	**-3.78**	**0.37**	**<0.01**	**0.52**
S_m	10.22	-0.08	0.00	0.77	0.79	0.30	-0.01	0.19	0.07	0.00	**86.75**	**3.30**	**0.35**	**<0.01**	**0.65**
stom/A_{leaf}	5.56	0.11	0.11	0.19	0.70	0.06	2.57e-3	0.13	0.14	0.00	120.80	-0.21	0.01	0.63	0.00
stom/SA_{mes}	5.83	1.05e+6	0.12	0.17	0.74	**0.01**	**3.93e+4**	**0.40**	**<0.01**	**0.00**	**163.10**	**-1.01e+7**	**0.43**	**<0.01**	**0.67**
stom/V_{IAS}	7.77	1.88e+6	0.14	0.14	0.52	**0.05**	**5.05e+4**	**0.29**	**<0.05**	**0.00**	**137.21**	**-1.09e+7**	**0.23**	**<0.05**	**0.00**
stom/V_{mes}	7.52	5.85e+6	0.04	0.43	0.71	**-6.36e-3**	**3.74e+5**	**0.44**	**<0.01**	**0.00**	**146.51**	**-7.38e+7**	**0.30**	**<0.05**	**0.00**
V_{BS+TT}/V_{leaf}	**6.13**	**49.65**	**0.38**	**<0.01**	**0.00**	0.10	0.37	0.07	0.27	0.00	112.90	-5.67	0.00	0.94	0.00
V_{ep}/V_{leaf}	4.99	33.27	0.04	0.46	0.77	-0.03	1.26	0.13	0.15	0.00	137.3	-164.4	0.04	0.44	0.00
V_{mes}/V_{leaf}	**48.62**	**-51.82**	**0.54**	**<0.001**	**0.00**	0.49	-0.51	0.17	0.08	0.00	85.25	41.84	0.02	0.57	0.00
V_{resin}/V_{leaf}	9.97	-35.45	0.00	0.74	0.78	0.20	-2.04	0.05	0.35	0.00	101.3	799.1	0.14	0.12	0.00
V_{vein}/V_{leaf}	8.68	28.85	0.00	0.77	0.79	0.18	-3.34	0.17	0.09	0.58	**93.19**	**1442.04**	**0.54**	**<0.001**	**0.63**
$V_{IAS/}$ stom	**24.74**	**-1.61e-5**	**0.44**	**<0.01**	**0.00**	**0.31**	**-2.58e-7**	**0.38**	**<0.01**	**0.00**	88.85	4.19e-05	0.17	0.09	0.00
$V_{mes/}$ stom	14.68	-1.57e-6	0.08	0.27	0.66	**0.33**	**-6.43e-8**	**0.39**	**<0.01**	**0.00**	85.35	1.04e-05	0.18	0.08	0.00

Supplementary Information References

1. G. Théroux-Rancourt *et al.*, Maximum CO2 diffusion inside leaves is limited by the scaling of cell size and genome size. *Proceedings of the Royal Society B: Biological Sciences* **288**, 20203145 (2021).